Water-Soluble Nanoparticles with Twisted Double [7]Carbohelicene for Lysosome-Targeted Cancer Photodynamic Therapy

Hao Zhao[1,3], Xiushang Xu[1], Long Zhou[2], Yunbin Hu[2], Yiming Huang[3], and Akimitsu Narita[1]*

H. Zhao, X. Xu, A. Narita
Organic and Carbon Nanomaterials Unit, Okinawa Institute of Science and Technology Graduate University, 1919-1 Tancha, Onna-son, Kunigami-gun, Okinawa 904-0495, Japan
E-mail: akimitsu.narita@oist.jp

L. Zhou, Y. Hu
College of Chemistry and Chemical Engineering, Central South University, Changsha, Hunan 410083, China

H. Zhao, Y. Huang
Key Laboratory of Organic Solids, Institute of Chemistry, Chinese Academy of Sciences, Beijing 100190, P. R. China

Keywords: carbohelicene, nanoparticle, bioimaging, photodynamic therapy, cancer treatment

Abstract: Helicene-based therapeutic agents for organelle-targeted photodynamic therapy (PDT) involving both type I and II is challenging and still underexplored. Herein, water-soluble nanoparticles containing twisted double [7]carbohelicene (D7H-NPs) are prepared through self-assembly with 1,2-distearoyl-sn-glycero-3-phosphoethanolamine-*N*-[methoxy(polyethylene glycol)-2000] (DSPE-PEG2000) by a nanoprecipitation method. D7H-NPs display high water-solubility with an average size of 46 ± 2 nm. Notably, D7H-NPs can generate efficient singlet oxygen ($^1O_2$) and superoxide anion ($O_2^{\cdot -}$) upon white light irradiation, forming the basis of PDT. Moreover, the typical accumulation in lysosomes of 4T1 cancer cells paves the way to utilize D7H-NPs for lysosome-targeted cancer phototherapeutics. This contribution reports a promising helicene-based phototherapeutic agent involving both type I and II PDT for organelle-targeted biotherapy.

1. Introduction

Photodynamic therapy (PDT) offers promising therapeutic opportunities to treat malignant tumors in a non-invasive manner with its high efficiency, low systemic toxicity, and minimal risks to cause drug resistance. [1-6] In PDT, photosensitizers (PSs) produce reactive oxygen species (ROS) under light excitation and lead to cancer cell death by causing vascular damage, inducing cell apoptosis, and activating immune reactions. [7-9] Specifically, PSs generate hydroxyl or superoxide radicals in type I PDT and singlet oxygen ($^1O_2$) in type II PDT under light irradiation. [10-12] Currently, type II PDT agents occupy the dominant position in cancer phototherapy by sensitizing oxygen into $^1O_2$, but its efficiency is severely limited by the insufficient oxygen supply inside hypoxia solid tumors. [13-15] Some efforts have been made to develop oxygen-supplying or oxygen-production systems to improve its concentration in the targeted areas, but complicated functional components and lab-operations are typically required. [16-19] Type I PDT that predominantly generates highly reactive radicals in a less oxygen-dependent manner is ideal for hypoxic tumor treatment. [20-21] A simple therapeutic agent that involves both type I and II PDT is anticipated to improve the treatment efficiency, which is highly desirable for cancer phototherapies, but photosensitizers with the relevant capability are still underdeveloped. [20-21]

Helicenes are polycyclic aromatic hydrocarbons (PAHs) with *ortho*-fused benzene rings and non-planar helical configurations. [22-25] Their characteristics of non-planarity, inherent chirality, and structural flexibility make them promising material candidates in the fields of molecular sensing, chiral optics, and organic (opto)electronics. [26-33] Additionally, some efforts have also been made for the development of helicene-based bioapplications. [34,35] For example, Tanaka *et al.* found that (*P*)-bis(dimethylaminomethyl)helicene displayed chiral selection in binding to left-handed Z-form DNA [36] while Lacour and coworkers investigated the mitochondria-targeted imaging abilities of cationic helicenes and [4]helicene-squalene nanoassemblies in living cells and *Chlamydomonas*. [37,38] Nevertheless, helicene-based

bioimaging is still rarely explored. Especially no organelle-targeted biotherapeutics with biocompatible helicenes or their derivatives have been reported up to now, to the best of our knowledge. On the other hand, it should be noted that the non-planarity of helicenes can reduce the aggregation caused by the strong π-π stacking, which is a typical problem of planar PAHs, thereby enhancing their solubility in organic solvents. However, their low water-solubility due to the hydrophobicity of the PAH structures strictly hampers their biological applications in aqueous media. [39-41] Development of simple and efficient synthesis of water-soluble helicene derivatives or direct water-solubilization of helicenes for biomedical applications still remains elusive.

Self-assembled nanoparticles (NPs) are proposed as a promising and feasible strategy to directly bring hydrophobic organic molecules into aqueous media and extensively used in biological applications. [42-46] Compared to the covalent functionalization of hydrophobic helicenes with hydrophilic substituents through the methods of synthetic organic chemistry, the nanoparticle strategies can circumvent complicated synthetic steps as well as often tedious separation and purification processes. [47] Additionally, the superiorities of the self-assembled NPs include outstanding biocompatibility and capability of the surface modification with various functional groups, which enable the targeting in the imaging, drug/gene delivery, and cancer cell killing. [47] The past decades have witnessed the booming developments of NP preparation methods including nanoprecipitation, [48-50] mini-emulsion, [51,52] and self-assembly [53,54]. Especially, the nanoprecipitation method is facile and highly versatile, and successfully employed for the preparations of NPs containing conjugated polymer, [47,55] fluorescent molecules with aggregation-induced emission, [46,56] and graphene quantum dots (GQDs), [57,58] allowing the applications in cell imaging, disease diagnosis, and therapeutics. Nevertheless, to the best of our knowledge, there are only a few reports on the preparation of NPs containing helicenes or other PAHs for such bioapplications. [59,60]

In this work, we fabricated water-soluble NPs containing twisted double [7]carbohelicene (D7H-NPs) with the aim of bioimaging and organelle-targeted biotherapeutic applications. As shown in **Scheme 1**, D7H-NPs were prepared through the nanoprecipitation method by reprecipitating D7H with amphiphilic 1,2-distearoyl-sn-glycero-3-phosphoethanolamine-*N*-[methoxy(polyethylene glycol)-2000] (DSPE-PEG2000). The resulting D7H-NPs displayed excellent water-solubility with an average size of 46 ± 2 nm. After incubating 4T1 cancer cells with D7H-NPs for 24 h, their accumulation was observed specifically in the lysosomes, implying their capability of organelle-targeted bioimaging. Moreover, efficient generation of singlet oxygen ($^1O_2$) and superoxide anion ($O_2^{\cdot-}$) was observed upon white light irradiation to D7H-NPs, which could be successfully applied to kill the 4T1 cancer cells. This contribution not only reports a promising helicene-based phototherapeutic agent involving both type I and II PDT, but also demonstrate a facile and direct way of making helicene water-soluble for organelle-targeted biotherapy.

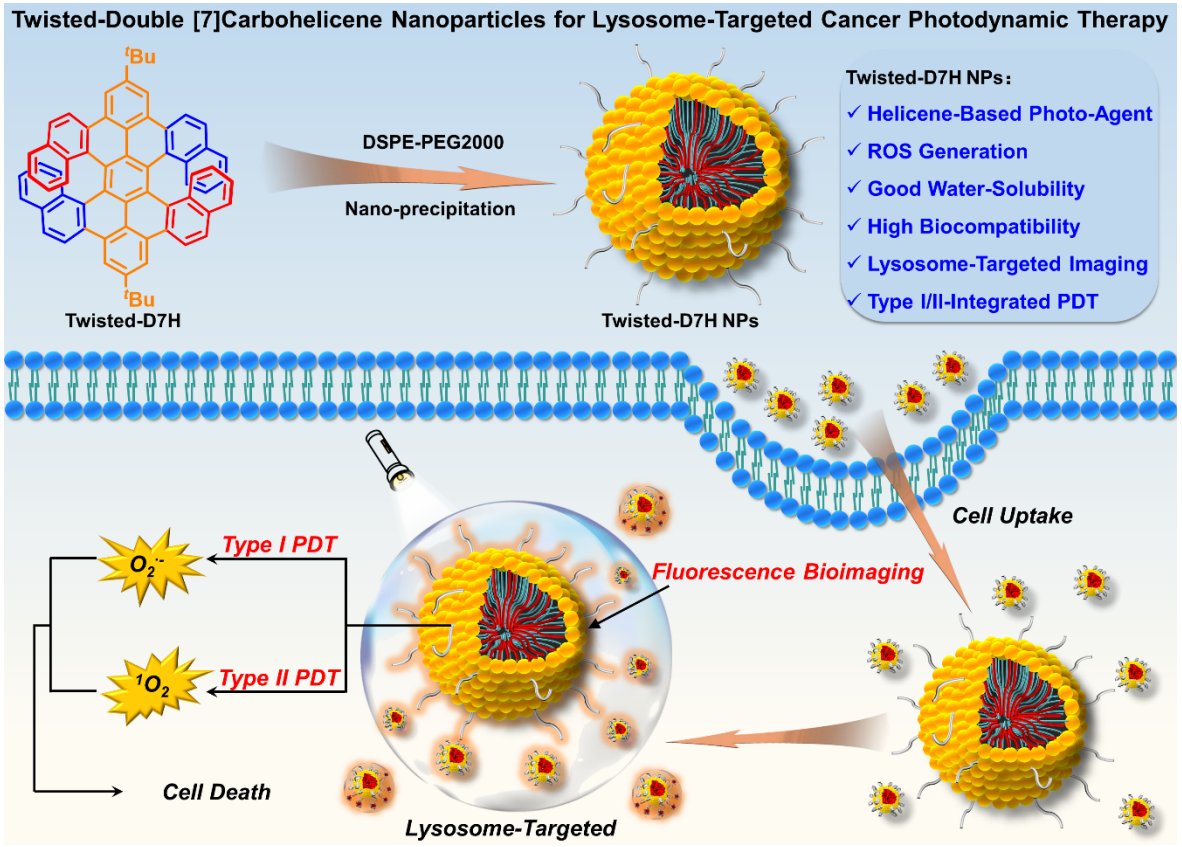

Scheme 1. Schematic illustration of water-soluble nanoparticles with twisted double [7]carbohelicene for lysosome-targeted cancer photodynamic therapy.

2. Results and Discussion

D7H was synthesized according to our previously reported procedure [26] and characterized by ^{1}H and ^{13}C NMR analyses (**Figure S1** and **S2**). As shown in **Figure 1a** and **Table S1**, the theoretically optimized configuration of the D7H molecule exhibits a twisted and non-planar conformation, which can suppress the aggregation caused by the strong π-π stacking. The highest occupied molecular orbital (HOMO), and the lowest unoccupied molecular orbital (LUMO) of D7H were theoretically calculated to be at –5.00 eV and –2.35 eV, respectively, with a HOMO-LUMO gap of 2.65 eV, which was consistent with the longest-wavelength absorption peak observed at 517 nm and a fluorescence peak at 574 nm when measured in tetrahydrofuran (THF), in line with our previous report [26].

As shown in the Jablonski diagram (**Figure 1b**), a photosensitizer is photoexcited from a ground state (S_0) to a singlet excited state (S_1), and then converts to a triplet excited state (T_1) through intersystem crossing (ISC). The energy of T_1 can subsequently sensitize surrounding oxygen to produce ROS. The $^{1}O_2$ generation ability of D7H was initially investigated in THF by using 1,3-diphenylisobenzofuran (DPBF) as a probe. As displayed in **Figure 1c**, the absorbance of DPBF at 415 nm decreased significantly upon white light irradiation in the presence of D7H, while the absorption spectra of D7H was not affected by the light irradiation (**Figure S3a-c**). A control experiment without D7H showed negligible changes upon the light irradiation, and these results indicated the photo-triggered $^{1}O_2$ generation sensitized by D7H. Notably, the $^{1}O_2$ generation ability was concentration-dependent, showing larger declines of the absorbance when increasing the concentration of D7H. The $^{1}O_2$ generation quantum yield of D7H was determined to be 0.67 using a commercial photosensitizer methylene blue (MB, 0.52) as a reference (**Figure S3d-f**). [61]

Electron spin resonance (ESR) analysis of a solution of D7H and 2,2,6,6-tetramethylpiperidine (TEMP) in dimethyl sulfoxide (DMSO) further corroborated the

generation of $^1O_2$ upon light irradiation, exhibiting a triplet signal indicative of $^1O_2$, [3] while showing no detectable signal in control experiments without D7H and/or light (**Figure 1d**). Moreover, ESR analysis of a solution of D7H and 5,5-dimethyl-1-pyrroline-*N*-oxide (DMPO) indicated the generation of superoxide anion ($O_2^{\cdot-}$) upon light irradiation (**Figure S4**), [62,63] presumably through the electron transfer from D7H in the triplet excited state to oxygen. [21] These findings suggested that D7H can be used as a powerful photosensitizer, which motivated us to prepare water-soluble nanoparticles with D7H and explore their bioapplications.

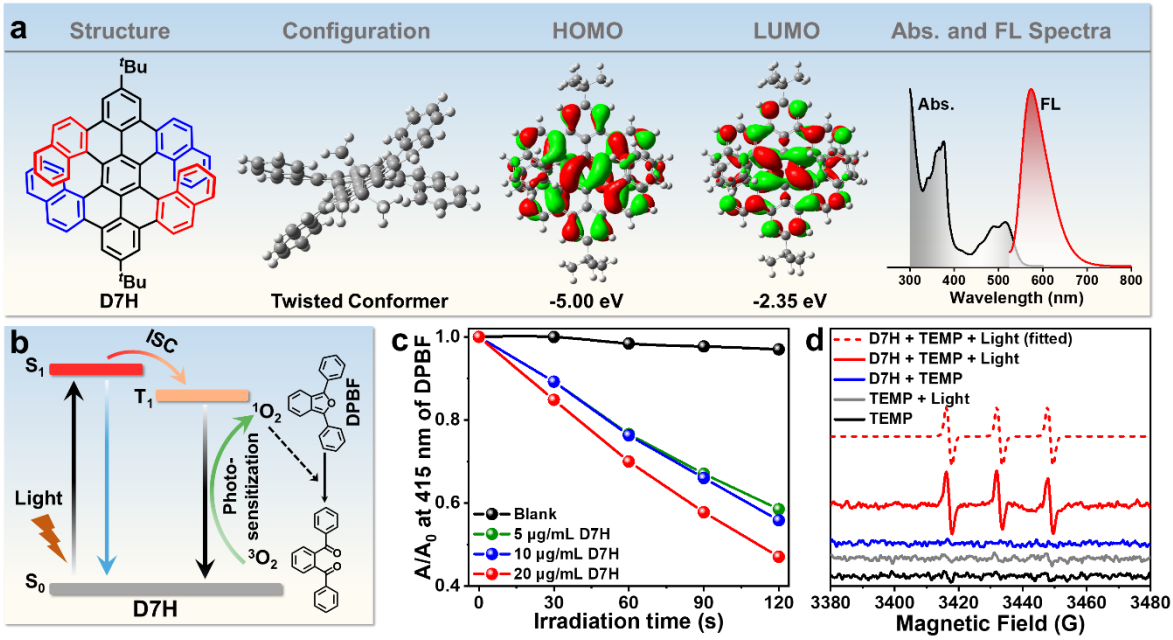

Figure 1. Theoretical calculation and photophysical and photosensitization studies of D7H in solution. (a) Chemical structure, theoretically optimized configuration, HOMO, LUMO, and absorption (Abs.) and fluorescence (FL) spectra of D7H in THF (20 μg/mL). λ_{ex} = 517 nm. (b) Proposed mechanism of photo-induced $^1O_2$ generation by D7H and $^1O_2$ detection with DPBF as the probe. (c) Concentration-dependent studies of the $^1O_2$ generation by D7H after different irradiation times in THF, based on the absorbance change of DPBF probe at 415 nm. (d) ESR spectra of TEMP in dark (black solid line), TEMP under light (grey solid line), D7H + TEMP in dark (blue solid line), and D7H + TEMP under light (red solid line) in DMSO and the fitted curve of D7H + TEMP under light (red dot line) using the instrument software.

D7H molecules were directly employed to prepare water-soluble nanoparticles, without any structural modification or covalent functionalization, for bioimaging and photodynamic anticancer applications. D7H-NPs were prepared by self-assembling hydrophobic D7H molecules with amphiphilic polymer DSPE-PEG2000 through the nanoprecipitation method

(**Figure 2a**). [64] D7H-NPs in water displayed similar absorption and fluorescence spectra to those of a solution of D7H in THF, forming yellowish, transparent dispersion without obvious aggregates visible to the naked eyes and emitting bright fluorescence under ultraviolet light irradiation (**Figure 2b**). Dynamic light scattering (DLS) analysis of D7H-NPs indicated an average diameter of 46 ± 2 nm with a small polydispersity index of 0.149, and transmission electron microscopy images displayed regular spherical morphology of the D7H-NPs with sizes in agreement with the DLS results (**Figures 2c** and **S5**). In addition, the zeta potential of D7H-NPs was measured to be –35 ± 3 mV, where the negative charge was ascribed to PEG chains on the surface of nanoparticles (**Figure 2d**). Notably, D7H-NPs maintained ~60% of their initial fluorescence intensity after irradiation by white light for 360 s (**Figure S6**), indicating their good photostability and suitability for the bioimaging application. The ROS generation ability of D7H-NPs under white light irradiation was evaluated with a probe of 2′,7′-dichlorofluorescin (DCFH), which can be oxidized to fluorescent 2′,7′-dichlorofluorescein (DCF) by ROS. The fluorescence intensity of DCFH significantly increased in the presence of D7H-NPs under white light irradiation as a function of irradiation time (**Figure 2f**). In contrast, the fluorescence intensity variations in the control experiments without D7H-NPs (DCFH + Light) or without DCFH (D7H-NPs + Light) were obviously lower or negligible. Additionally, the typical ESR spectra of D7H-NPs + TEMP + Light and D7H-NPs + DMPO + Light further confirmed the production of $^1O_2$ and $O_2^{\cdot -}$ by D7H-NPs in water under light irradiation (**Figure 2g** and **2h**). [3,62,63] The ROS generation efficiency of D7H-NPs was very similar to D7H molecules in solution (**Figure 1d** and **S4**), reinforcing the potential of D7H-NPs as powerful photosensitizers in aqueous environments.

Subsequently, the absorption and fluorescence spectra, absolute fluorescence quantum yield and lifetime of D7H in THF, D7H molecules dispersed in water and D7H-NPs in water were investigated. As shown in **Figure S7**, D7H-NPs exhibited a very similar absorption spectrum to that of D7H dissolved in THF, suggesting the absence of strong intermolecular

interactions between D7H molecules inside the D7H-NPs in water. In contrast, the absorption spectra of D7H dispersed in water displayed a redshift of the absorption maximum from 520 nm to 525 nm and broadening, which could be ascribed to aggregation-induced effects. Besides, the absolute fluorescence quantum yield of D7H in THF was 19.6%, while that of D7H dispersed in water was only 6.4% and it was partly recovered to 13.1% for D7H-NPs (**Figure 2i**). Moreover, the average fluorescence lifetime of D7H in THF, D7H dispersed in water, and D7H-NPs in water were respectively determined to be 9.17 ns, 1.40 ns, and 10.86 ns (**Figure 2j**). All these findings confirmed that D7H-NPs were well water-soluble and could retain the photophysical properties of D7H molecules to the great extent, suppressing the detrimental intermolecular interactions, which highlighted the advantage of the nanoparticle method to directly bring hydrophobic helicene molecules into water without additional synthetic efforts.

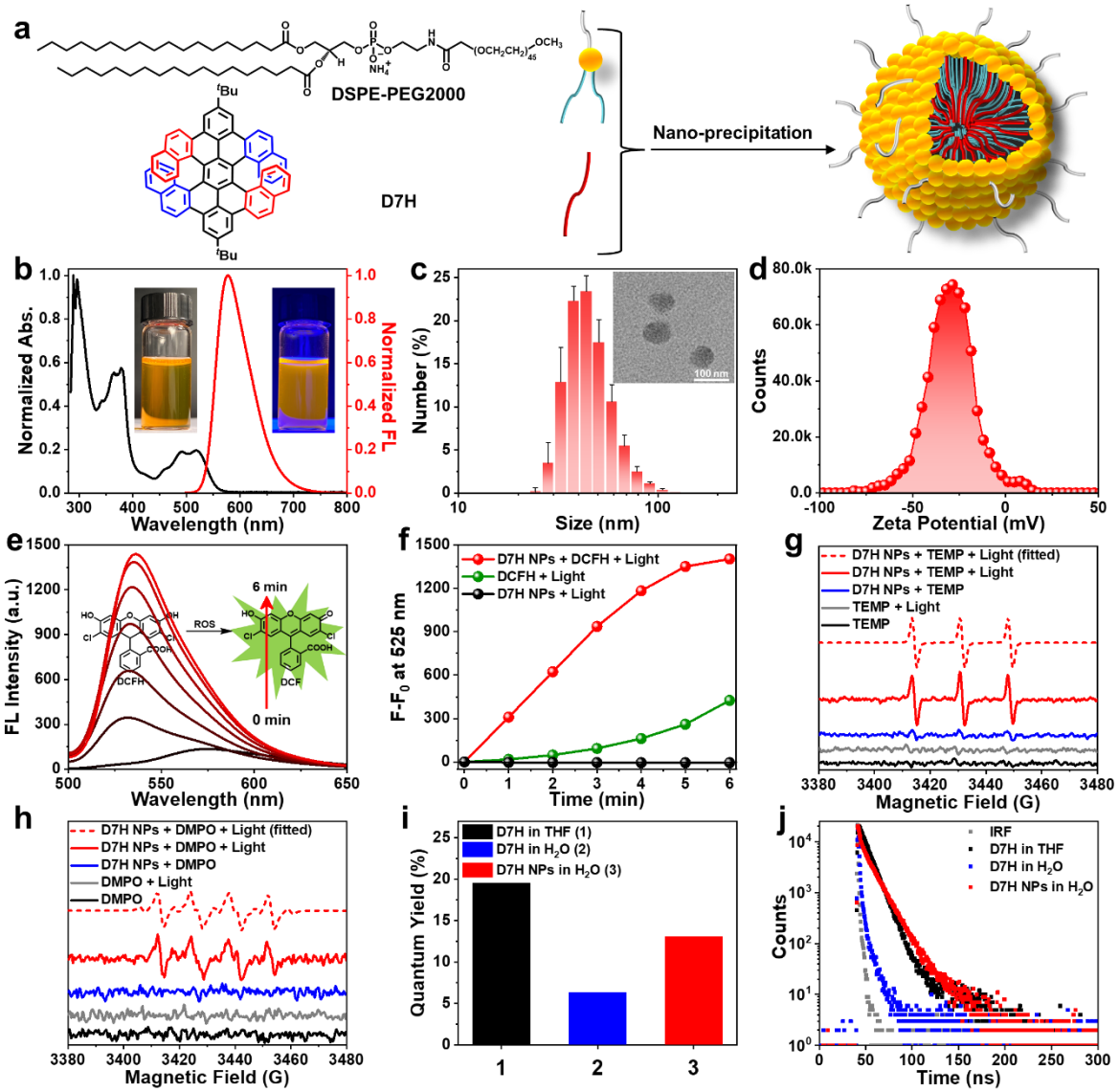

Figure 2. Preparation and characterizations of D7H-NPs. (a) Schematic illustration of the preparation process of D7H-NPs by a nanoprecipitation method. (b) Normalized absorption and fluorescence spectra of D7H-NPs in water (100 μg/mL, based on the weight of D7H without DSPE-PEG2000). Inset: photographs of D7H solution with (right) and without (left) UV light irradiation. (c) Size distribution of D7H-NPs by DLS experiments. Inset: TEM image of D7H-NPs. (d) Zeta potential of D7H-NPs in water. (e) Fluorescence spectra of DCFH solution containing D7H-NPs (20 μg/mL) under white light irradiation (20 mW/cm^2). Inset: the mechanism of fluorescence recovery of DCFH solution triggered by ROS. (f) The fluorescence intensity increments at 525 nm of D7H-NPs + DCFH (red solid line), DCFH (green solid line), and D7H-NPs (black solid line) under light irradiation in water. (g) ESR spectra of TEMP in dark (black solid line), TEMP under light (grey solid line), D7H-NPs + TEMP in dark (blue solid line), and D7H-NPs + TEMP under light (red solid line) in water, and the fitted curve of D7H-NPs + TEMP under light (red dot line) using the instrument software. (h) ESR spectra of DMPO in dark (black solid line), DMPO under light (grey solid line), D7H-NPs + DMPO in dark (blue solid line), and D7H-NPs + DMPO under light (red solid line) in water, and the fitted curve of D7H-NPs + DMPO under light (red dot line) using the instrument software. (i) The absolute fluorescence quantum yields and (j) fluorescence lifetime analyses of D7H in THF (20 μg/mL), D7H in water (20 μg/mL) and D7H-NPs in water (20 μg/mL based on the weight of D7H). IRF is the instrument response function.

The excellent water-solubility, reasonable fluorescence quantum yield, and efficient photosensitization ability of D7H-NPs provide a promising opportunity for its bioimaging and anticancer applications in PDT. The cellular biocompatibility of D7H-NPs was evaluated with a standard 3-(4,5-dimethylthiazol-2-yl)-2,5-diphenyltetrazolium bromide (MTT) assay. [3] As displayed in **Figure S8**, 4T1 cells kept high cell viability when the concentration of D7H-NPs was as high as 10 μg/mL (based on the weight of D7H), which was also applied as the optimized work concentration in the following investigations. When incubating with 4T1 cancer cells, the signal of D7H-NPs steadily increased in the confocal laser scanning microscopy (CLSM) images, indicating that D7H-NPs were gradually internalized, which was completed after 24 hours (**Figure S9**). The intracellular distribution of D7H-NPs was subsequently investigated by cell co-localization analysis with DAPI (cell nucleus dye), DiD (cell membrane dye), MitoTracker, and LysoTracker by CLSM after incubating with 4T1 cancer cell for 24 h. As shown in **Figure 3a**, D7H-NPs were located in the cell cytoplasm outside the cell nucleus. Line series analysis indicated the signal of D7H-NPs between the signals of DiD in the surrounding cell membranes (**Figure 3b**). On the other hand, the green fluorescence of D7H-NPs did not overlap with the red fluorescence of Mito Tracker, and presented their individual signals in the merged image (**Figure 3a** and **3c**). In contrast, D7H-NPs overlapped very well with LysoTracker and displayed a yellowish signal in the merged image (**Figure 3a**), implying that D7H-NPs mainly accumulated in the lysosomes rather than the mitochondria. Line series analysis of CLSM images further corroborated the distribution of D7H-NPs in the lysosomes with the help of the synchronous fluorescence intensity variations (**Figure 3d**). It should be noted that D7H-NPs were prepared without specific surface functionalization, and thus they were most probably internalized into cells by forming early endosomes, which would be eventually located in late endosomes and lysosomes. [1] These results suggested that D7H-NPs could specifically accumulate in the lysosomes of 4T1 cancer cells, highlighting its lysosome-targeted bioimaging ability.

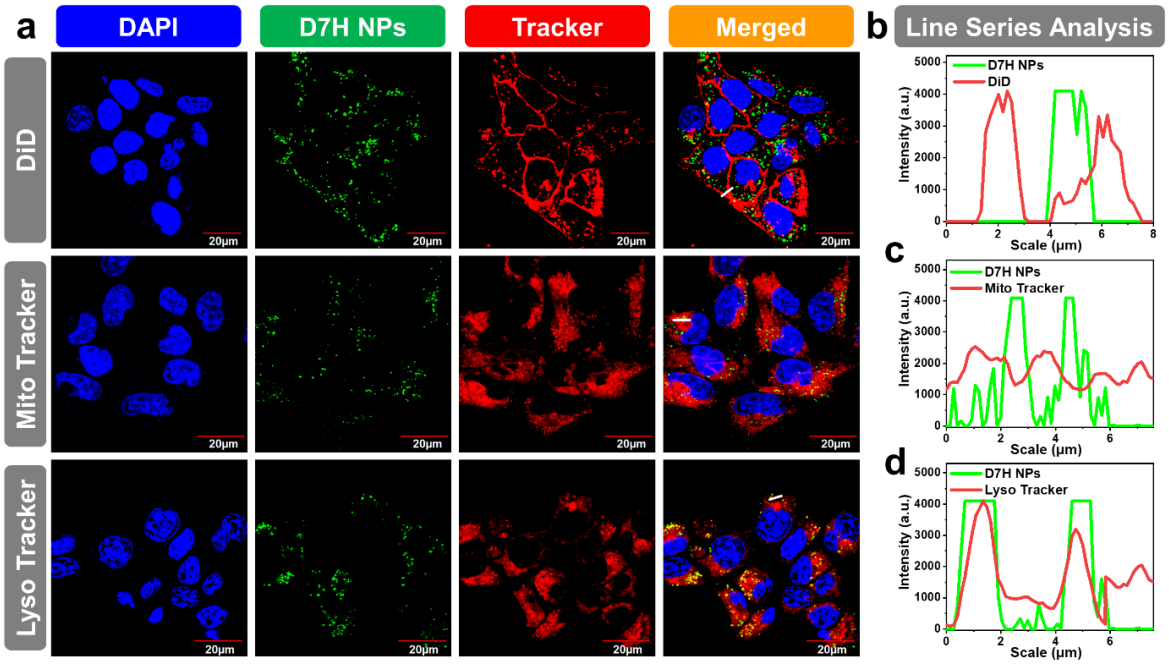

Figure 3. Cell co-localization analysis of D7H-NPs in 4T1 cancer cells. (a) Co-localization of D7H-NPs with DAPI (cell nucleus dye), DiD (cell membrane dye), MitoTracker, and LysoTracker after incubating with 4T1 cancer cells for 24 h. Scale bar: 20 μm. Line series analysis of D7H-NPs with (b) DiD, (c) MitoTracker, and (d) LysoTracker. The colors shown in the images are all false colors; blue: cell nucleus, green: D7H-NPs, and red: DiD or MitoTracker or LysoTracker. The fluorescence of DAPI, D7H-NPs, and DiD/MitoTracker/LysoTracker was collected in the ranges of 420–460 nm (λ_{ex}: 405 nm), 500–600 nm (λ_{ex}: 488 nm) and 660–700 nm (λ_{ex}: 633 nm), respectively.

The anticancer effect of D7H-NPs in PDT was subsequently investigated on 4T1 cancer cells. Intracellular ROS production of D7H-NPs under white light irradiation was explored with a probe of 2′,7′-dichlorodihydrofluorescein diacetate (DCFH-DA). As illustrated in **Figure 4a**, 4T1 cells incubated with DCFH-DA emitted obvious green fluorescence in the presence of D7H-NPs under white light irradiation, verifying the successful intracellular ROS production. In contrast, negligible fluorescence was detected in the cells without light and/or D7H-NPs. Besides, the viabilities of 4T1 cells gradually decreased with increasing concentration of D7H-NPs under white light irradiation, while the cells incubated with D7H-NPs kept high cell survival rates without the light irradiation, which reflected a good anticancer efficiency in PDT and promising biocompatibility of D7H-NPs (**Figure 4b**). The PDT killing effect was further verified by live/dead cell staining assay. As demonstrated in **Figure 4c**, most of the cells in the group of D7H-NPs with the irradiation were dead and stained by propidium iodide (PI),

emitting red fluorescence. However, the cells in three other control groups without D7H-NPs and/or the light irradiation showed green fluorescence from calcein AM (AM), indicating their living state after the treatments and highlighting the outstanding biocompatibility of D7H-NPs. As exhibited in **Figure 4b**, the cell viability decreased to be 27.8% after treatment with 10 μg/mL D7H-NPs under white light irradiation (20 mW/cm^2 for 20 min). The anticancer efficiency of D7H-NPs is thus higher than that of NPs with benzo[*c*]thiophene-based organic molecule (BT-NPs, ~80% cell viability under the concentration of 12 μg/mL, 655 nm laser (1 W/cm^2) irradiation for 5 min).[3] This result is also comparable to previous reports on NPs with conjugated polymer, poly(fluorene-*co*-vinylene) (PFV-NPs, ~24.6% cell viability under the concentration of 10 μg/mL, white light (25 mW/cm^2) irradiation for 30 min) [65] as well as NPs with typical aggregation-induced emission molecule, tetraphenylethylene (TPETS-NPs, ~25% cell viability under the concentration of 10 μg/mL, 450 nm light (250 mW/cm^2) irradiation for 3 min) [66]. Besides, the BT-NPs, PFV-NPs and TPETS-NPs all displayed type II PDT effect showing successful generation of $^1O_2$ but the generation of $O_2^{\cdot-}$ through type I PDT was not demonstrated, in contrast to D7H-NPs that could produce both $^1O_2$ and $O_2^{\cdot-}$ under white light irradiation through type I and II mechanisms. Compared with other reported photosensitizers, the characteristics of the π-conjugated helicene system could presumably also promote the singlet to triplet intersystem crossing through the large spin-orbit coupling, thereby augmenting the photosensitization efficiency.[67] The $^1O_2$ generation quantum yield of D7H was determined to be 0.67, which is higher than the those of the widely used photosensitizers MB (0.52), Eosin Y (0.60), Eosin B (0.37), and 5,10,15,20-tetrakis(4-sulfonatophenyl)porphine (H_2TPPS^{4-}, 0.6).[68] These results solidly reinforced the superiorities of D7H-NPs as a promising helicene-based photosensitization agent involving both type I and II PDT effects.

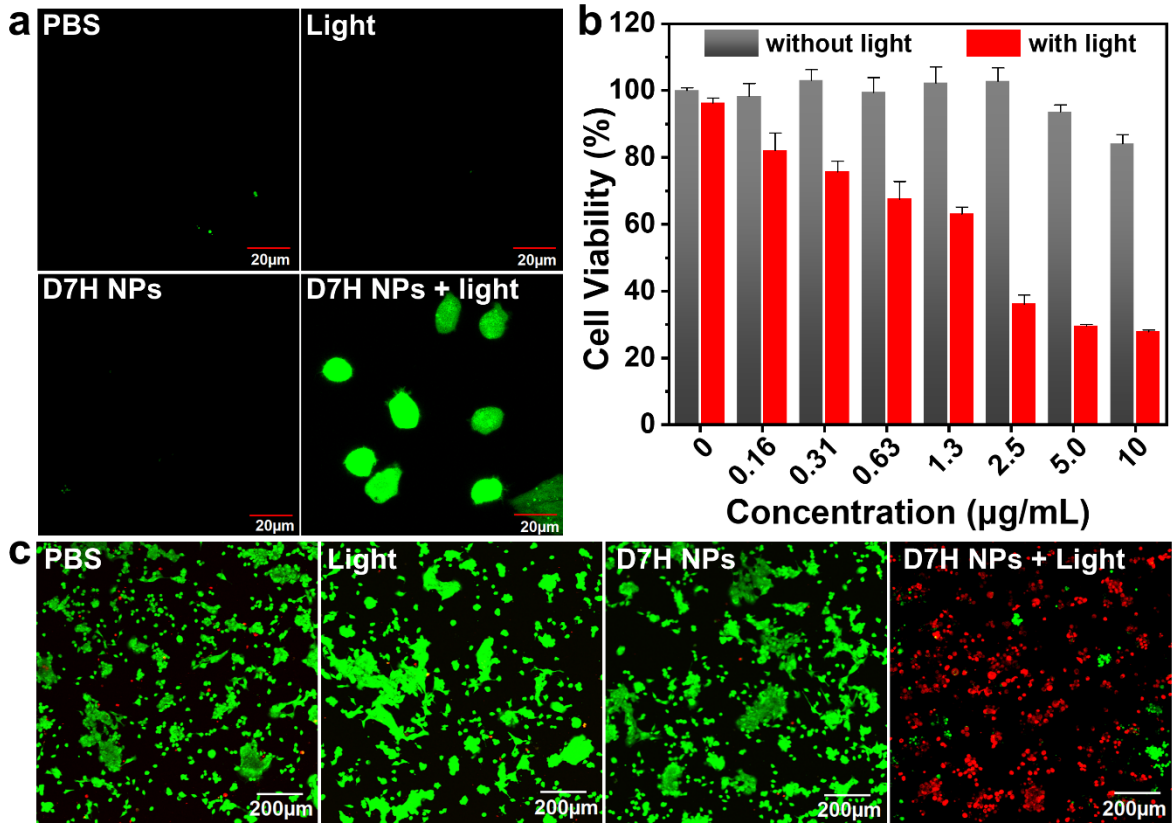

Figure 4. Intracellular ROS generation and cytotoxicity of D7H-NPs to 4T1 cancer cells. (a) CLSM imaging of intracellular ROS generation in 4T1 cancer cells treated with only PBS, light, D7H-NPs, and D7H-NPs + light. The fluorescence was collected at the range of 500–540 nm (λ_{ex}: 488 nm). (b) Viability of 4T1 cancer cells treated with various concentrations of D7H-NPs with or without white light irradiation for 20 min (20 mW/cm^2). (c) CLSM images of 4T1 cancer cells costained with AM (green fluorescence for live cells) and PI (red fluorescence for dead cells) after different treatments. The fluorescence of AM and PI were collected at the ranges of 500–540 nm (λ_{ex}: 488 nm) and 570–650 nm (λ_{ex}: 559 nm), respectively.

3. Conclusion

In summary, we achieved the preparation of water-soluble D7H-NPs with hydrophobic double [7]carbohelicene by the nanoprecipitation method and their application for lysosome-targeted bioimaging and photodynamic therapy of cancer cells. D7H-NPs in water possessed similar photophysical properties to D7H molecules in solution, efficiently suppressing the detrimental aggregation-induced effects. Moreover, D7H-NPs specifically accumulated in the lysosomes of 4T1 cells, and generated reactive species (e.g. $^1O_2$ and $O_2^{\cdot-}$) under light excitation followed by inducing cancer cell apoptosis. These results highlight the potential of D7H-NPs as a promising helicene-based organelle-targeted phototherapeutic agent involving type I and II PDT. Moreover, this work opens up a new avenue toward the use of the chiral nature of

helicenes in bioapplications, such as functional DNA, protein or other natural receptor-targeted PDT through the enantioselective recognition.

Supporting Information

Supporting Information is available from the Wiley Online Library or from the author.

Acknowledgements

This work was supported by the Okinawa Institute of Science and Technology Graduate University (OIST) and JSPS KAKENHI Grant Number JP19K24686. Y. Hu. acknowledges the financial support from the National Natural Science Foundation (21901257) and Innovation-Driven Project of Central South University (502501009). We would like to thank Prof. Shu Wang at Institute of Chemistry, Chinese Academy of Sciences for providing the access to the scientific facilities, and appreciate Prof. Klaus Müllen at the Max Planck Institute for Polymer Research for his insightful advises and discussions. We also appreciate help and support provided by the Scientific Computing and Data Analysis Section of Research Support Division at OIST.

Received: ((will be filled in by the editorial staff))
Revised: ((will be filled in by the editorial staff))
Published online: ((will be filled in by the editorial staff))

References

[1] C. Zhu, L. Liu, Q. Yang, F. Lv, S. Wang, *Chem. Rev.* **2012**, *112*, 4687.

[2] H. Chen, S. Li, M. Wu, Kenry, Z. Huang, C.-S. Lee, B. Liu, *Angew. Chem., Int. Ed.* **2020**, *59*, 632.

[3] Y. Wan, G. Lu, W.-C. Wei, Y.-H. Huang, S. Li, J.-X. Chen, X. Cui, Y.-F. Xiao, X. Li, Y. Liu, X.-M. Meng, P. Wang, H.-Y. Xie, J. Zhang, K.-T. Wong, C.-S. Lee, *ACS Nano* **2020**, *14*, 9917.

[4] N. M. Idris, M. K. Gnanasammandhan, J. Zhang, P. C. Ho, R. Mahendran, Y. Zhang, *Nat. Med.* **2012**, *18*, 1580.

[5] Z. Yang, X. Chen, *Acc. Chem. Res.* **2019**, *52*, 1245.

[6] K. Yamagishi, I. Kirino, I. Takahashi, H. Amano, S. Takeoka, Y. Morimoto, T. Fujie, *Nat. Biomed. Eng.* **2019**, *3*, 27.

[7] J. P. Celli, B. Q. Spring, I. Rizvi, C. L. Evans, K. S. Samkoe, S. Verma, B. W. Pogue, T. Hasan, *Chem. Rev.* **2010**, *110*, 2795.

[8] D. E. J. G. J. Dolmans, D. Fukumura, R. K. Jain, *Nat. Rev. Cancer* **2003**, *3*, 380.

[9] B. Yang, Y. Chen, J. Shi, *Chem. Rev.* **2019**, *119*, 4881.

[10] J. Yao, Y. Cheng, M. Zhou, S. Zhao, S. Lin, X. Wang, J. Wu, S. Li, H. Wei, *Chem. Sci.* **2018**, *9*, 2927.

[11] L. Benov, *Protoplasma* **2001**, *217*, 33.

[12] H. Lu, X. Jiang, Y. Chen, K. Peng, Y. Huang, H. Zhao, Q. Chen, F. Lv, L. Liu, S. Wang, Y. Ma, *Nanoscale* **2020**, *12*, 14061.

[13] Q. Chen, L. Feng, J. Liu, W. Zhu, Z. Dong, Y. Wu, Z. Liu, *Adv. Mater.* **2016**, *28*, 7129.

[14] H. S. Jung, J. Han, H. Shi, S. Koo, H. Singh, H.-J. Kim, J. L. Sessler, J. Y. Lee, J.-H. Kim, J. S. Kim, *J. Am. Chem. Soc.* **2017**, *139*, 7595.

[15] J. Liu, W. Bu, J. Shi, *Chem. Rev.* **2017**, *117*, 6160.

[16] L. Jiang, H. Bai, L. Liu, F. Lv, X. Ren, S. Wang, *Angew. Chem., Int. Ed.* **2019**, *58*, 10660.

[17] J. Ouyang, L. Wang, W. Chen, K. Zeng, Y. Han, Y. Xu, Q. Xu, L. Deng, Y.-N. Liu, *Chem. Commun.* **2018**, *54*, 3468.

[18] T.-J. Zhou, L. Xing, Y.-T. Fan, P.-F. Cui, H.-L. Jiang, *J. Control. Release* **2019**, *307*, 44.

[19] D. Zheng, B. Li, L. Xu, Q.-L. Zhang, J.-X. Fan, C.-X. Li, X.-Z. Zhang, *ACS Nano* **2018**, *12*, 6218.

[20] M. Li, T. Xiong, J. Du, R. Tian, M. Xiao, L. Guo, S. Long, J. Fan, W. Sun, K. Shao, X. Song, J. W. Foley, X. Peng, *J. Am. Chem. Soc.* **2019**, *141*, 2695.

[21] a) M. Li, J. Xia, R. Tian, J. Wang, J. Fan, J. Du, S. Long, X. Song, J. W. Foley, X. Peng, *J. Am. Chem. Soc.* **2018**, *140*, 14851; b) D. Chen, Q. Xu, W. Wang, J. Shao, W. Huang, X. Dong, *Small* **2021**, *17*, 2006742.

[22] M. Gingras, *Chem. Soc. Rev.* **2013**, *42*, 968.

[23] M. Gingras, G. Félix, R. Peresutti, *Chem. Soc. Rev.* **2013**, *42*, 1007.

[24] M. Gingras, *Chem. Soc. Rev.* **2013**, *42*, 1051.

[25] Y. Shen, C.-F. Chen, *Chem. Rev.* **2012**, *112*, 1463.

[26] Y. Hu, X.-Y. Wang, P.-X. Peng, X.-C. Wang, X.-Y. Cao, X. Feng, K. Müllen, A. Narita, *Angew. Chem., Int. Ed.* **2017**, *56*, 3374.

[27] Z. Zhou, L. Fu, Y. Hu, X.-Y. Wang, Z. Wei, A. Narita, K. Müllen, M. A. Petrukhina, *Angew. Chem., Int. Ed.* **2020**, *59*, 15923.

[28] B. J. Coe, D. Rusanova, V. D. Joshi, S. Sánchez, J. Vávra, D. Khobragade, L. Severa, I. Císařová, D. Šaman, R. Pohl, K. Clays, G. Depotter, B. S. Brunschwig, F. Teplý, *J. Org. Chem.* **2016**, *81*, 1912.

[29] Q. Huang, L. Jiang, W. Liang, J. Gui, D. Xu, W. Wu, Y. Nakai, M. Nishijima, G. Fukuhara, T. Mori, Y. Inoue, C. Yang, *J. Org. Chem.* **2016**, *81*, 3430.

[30] M. Ren, J. Wang, X. Xie, J. Zhang, P. Wang, *ACS Energy Lett.* **2019**, *4*, 2683.

[31] T. R. Schulte, J. J. Holstein, G. H. Clever, *Angew. Chem., Int. Ed.* **2019**, *58*, 5562.

[32] M. Stöhr, S. Boz, M. Schär, M.-T. Nguyen, C. A. Pignedoli, D. Passerone, W. B. Schweizer, C. Thilgen, T. A. Jung, F. Diederich, *Angew. Chem., Int. Ed.* **2011**, *50*, 9982.

[33] G. Zhang, J. Tan, L. Zhou, C. Liu, J. Liu, Y. Zou, A. Narita, Y. Hu, *Org. Lett.* **2021**, *23*, 6183.

[34] S. Liu, M. Bae, L. Hao, J. K. Oh, A. R. White, Y. Min, L. Cisneros-Zevallos, M. Akbulut, *Nanomaterials* **2021**, *11*, 89.

[35] K.-P. Wang, Y. Lei, Y. Sun, Q. Zhang, S. Chen, Q. Zhang, H.-Y. Hu, Z.-Q. Hu, *Sensors Actuators B Chem.* **2018**, *273*, 1487.

[36] Y. Xu, Y. X. Zhang, H. Sugiyama, T. Umano, H. Osuga, K. Tanaka, *J. Am. Chem. Soc.* **2004**, *126*, 6566.

[37] A. Babič, S. Pascal, R. Duwald, D. Moreau, J. Lacour, E. Allémann, *Adv. Funct. Mater.* **2017**, *27*, 1701839.

[38] C. Bauer, R. Duwald, G. M. Labrador, S. Pascal, P. Moneva Lorente, J. Bosson, J. Lacour, J.-D. Rochaix, *Org. Biomol. Chem.* **2018**, *16*, 919.

[39] J. Wu, W. Pisula, K. Müllen, *Chem. Rev.* **2007**, *107*, 718.

[40] J. Wu, J. Li, U. Kolb, K. Müllen, *Chem. Commun.* **2006**, 48.

[41] H.-A. Lin, Y. Sato, Y. Segawa, T. Nishihara, N. Sugimoto, L. T. Scott, T. Higashiyama, K. Itami, *Angew. Chem., Int. Ed.* **2018**, *57*, 2874.

[42] D.-E. Lee, H. Koo, I.-C. Sun, J. H. Ryu, K. Kim, I. C. Kwon, *Chem. Soc. Rev.* **2012**, *41*, 2656.

[43] J. Rauch, W. Kolch, S. Laurent, M. Mahmoudi, *Chem. Rev.* **2013**, *113*, 3391.

[44] M. Ha, J.-H. Kim, M. You, Q. Li, C. Fan, J.-M. Nam, *Chem. Rev.* **2019**, *119*, 12208.

[45] N. Panwar, A. M. Soehartono, K. K. Chan, S. Zeng, G. Xu, J. Qu, P. Coquet, K.-T. Yong, X. Chen, *Chem. Rev.* **2019**, *119*, 9559.

[46] H.-B. Cheng, Y. Li, B. Z. Tang, J. Yoon, *Chem. Soc. Rev.* **2020**, *49*, 21.

[47] L. Feng, C. Zhu, H. Yuan, L. Liu, F. Lv, S. Wang, *Chem. Soc. Rev.* **2013**, *42*, 6620.

[48] C. Wu, Y. Jin, T. Schneider, D. R. Burnham, P. B. Smith, D. T. Chiu, *Angew. Chem., Int. Ed.* **2010**, *49*, 9436.

[49] C. Wu, T. Schneider, M. Zeigler, J. Yu, P. G. Schiro, D. R. Burnham, J. D. McNeill, D. T. Chiu, *J. Am. Chem. Soc.* **2010**, *132*, 15410.

[50] a) C. Wu, S. J. Hansen, Q. Hou, J. Yu, M. Zeigler, Y. Jin, D. R. Burnham, J. D. McNeill, J. M. Olson, D. T. Chiu, *Angew. Chem., Int. Ed.* **2011**, *50*, 3430; b) Z. Cheng, T. Zhang, W. Wang, Q. Shen, Y. Hong, J. Shao, X. Xie, Z. Fei, X. Dong, *Chinese Chem. Lett.* **2021**, *32*, 1580.

[51] K. Li, J. Pan, S.-S. Feng, A. W. Wu, K.-Y. Pu, Y. Liu, B. Liu, *Adv. Funct. Mater.* **2009**, *19*, 3535.

[52] P. Howes, M. Green, J. Levitt, K. Suhling, M. Hughes, *J. Am. Chem. Soc.* **2010**, *132*, 3989.

[53] C. Xing, Q. Xu, H. Tang, L. Liu, S. Wang, *J. Am. Chem. Soc.* **2009**, *131*, 13117.

[54] G. Yang, L. Liu, Q. Yang, F. Lv, S. Wang, *Adv. Funct. Mater.* **2012**, *22*, 736.

[55] Y. Wang, L. Feng, S. Wang, *Adv. Funct. Mater.* **2019**, *29*, 1806818.

[56] X. Cai, B. Liu, *Angew. Chem., Int. Ed.* **2020**, *59*, 9868.

[57] J. Ge, M. Lan, B. Zhou, W. Liu, L. Guo, H. Wang, Q. Jia, G. Niu, X. Huang, H. Zhou, X. Meng, P. Wang, C.-S. Lee, W. Zhang, X. Han, *Nat. Commun.* **2014**, *5*, 4596.

[58] H. Wang, D. Yu, J. Fang, Y. Zhou, D. Li, Z. Liu, J. Ren, X. Qu, *Chem. Sci.* **2020**, *11*, 12721.

[59] C. Zhang, Y. Liu, X.-Q. Xiong, L.-H. Peng, L. Gan, C.-F. Chen, H.-B. Xu, *Org. Lett.* **2012**, *14*, 5912.

[60] J. Yu, Y. Chen, Y.-H. Zhang, X. Xu, Y. Liu, *Org. Lett.* **2016**, *18*, 4542.

[61] S. S. Khatoon, Y. Chen, H. Zhao, F. Lv, L. Liu, S. Wang, *Biomater. Sci.* **2020**, *8*, 2156.

[62] Y. Bando, K. Aki, *J. Biochem.* **1991**, *109*, 450.

[63] M. Kohno, Y. Mizuta, M. Kusai, T. Masumizu, K. Makino, *Bull. Chem. Soc. Jpn.* **1994**, *67*, 1085.

[64] Y.-F. Xiao, C. Xiang, S. Li, C. Mao, H. Chen, J.-X. Chen, S. Tian, X. Cui, Y. Wan, Z. Huang, X. Li, X.-H. Zhang, W. Guo, C.-S. Lee, *Small* **2020**, *16*, 2002672.

[65] Z. Lu, Z. Zhang, Y. Tang, *ACS Appl. Bio Mater.* **2019**, *2*, 4485.

[66] Y. Gao, Q. C. Zheng, S. Xu, Y. Yuan, X. Cheng, S. Jiang, Kenry, Q. Yu, Z. Song, B. Liu, M. Li, *Theranostics* **2019**, *9*, 1264.

[67] K. Dhbaibi, L. Favereau, J. Crassous, *Chem. Rev.* **2019**, *119*, 8846.

[68] F. Wilkinson, W. P. Helman, A. B. Ross. *J. Phys. Chem. Ref. Data* **1993**, *22*. 113.

Water-soluble nanoparticles containing twisted double [7]carbohelicene (D7H-NPs) are prepared for lysosome-targeted cancer treatment involving both type I and II photodynamic therapy. This contribution reports a promising helicene-based phototherapeutic agent involving both type I and II PDT for organelle-targeted biotherapy.

H. Zhao, X. Xu, L. Zhou, Y. Hu, Y. Huang, and A. Narita*

Water-Soluble Nanoparticles with Twisted Double [7]Carbohelicene for Lysosome-Targeted Cancer Photodynamic Therapy